Research Article

Combustion synthesis of Hf-doped zirconolite-rich composite waste forms and the aqueous durability

Kuibao ZHANG[a,b,*], Dan YIN[a], Zongsheng HE[a], Baozhu LUO[a], Haibin ZHANG[c]

[a]*State Key Laboratory of Environment-friendly Energy Materials, Southwest University of Science and Technology, Mianyang 621010, China*
[b]*National Defense Key Discipline Lab of Nuclear Waste and Environmental Safety, Southwest University of Science and Technology, Mianyang 621010, China*
[c]*Institute of Nuclear Physics and Chemistry, China Academy of Engineering Physics, Mianyang 621900, China*

Abstract: Zirconolite is recognized as one of the most durable waste matrices for the disposal of high-level radioactive wastes (HLWs). In this study, HfO_2 was employed as the surrogate of tetravalent actinides. Hf-bearing zirconolite-based composite waste forms ($CaZr_{1-x}Hf_xTi_2O_7$) were rapidly prepared by combustion synthesis (CS) using CuO as the oxidant, where quick pressing (QP) was introduced to obtain densified samples. Similar as solid state reaction process, the Zr site of zirconolite can be totally occupied by Hf ($x = 1.0$) under the CS reaction. The original 2M zirconolite structure was maintained and a small amount of perovskite impurity phase was generated in the final products. The aqueous durability of representative sample (Cu-Hf-0.6) was tested, where the 42-day normalized leaching rates (LR_i) of Ca, Cu, and Hf are 0.25, 3.10×10^{-2}, and 1.11×10^{-8} $g \cdot m^{-2} \cdot d^{-1}$.

Keywords: combustion synthesis (CS); nuclear waste; HfO_2; zirconolite; aqueous durability

1 Introduction

The disposal of high-level radioactive wastes (HLWs) has long been a great and urgent challenge for the nuclear industry [1,2]. Due to the long term radiotoxicity of minor actinides (MA, such as Np, Am, Cm, etc.) recovered from spent fuel reprocessing, the separation of these actinides and their final disposal in durable matrices are of prime importance. Advanced materials can enable enhanced performances of nuclear waste forms with promoted safety margins and chemical flexibility [3]. Vitrification using borosilicate or phosphate

glasses is generally recognized as the first generation waste management method. In recent decades, highly durable ceramic materials have been proposed as an alternative medium for HLW immobilization [4–6]. The naturally existed zirconolite and pyrochlore are important actinide-bearing ceramic materials, which exhibit excellent chemical and physical durability over geological time scales [7–12]. Zirconolite (ideally $CaZrTi_2O_7$) was also developed as a crystalline phase to sequester Pu from surplus nuclear weapons, which makes it receive great attention as a potential waste form [13].

Zirconolite is formed by the stacking layers of edge shared Ti–O polyhedra (TiO_5 and TiO_6) and layers of Ca^{2+} and Zr^{4+} cations [14]. Due to that the Ti^{4+} and Zr^{4+} ions can be mutually occupied, the zirconolite

---

* Corresponding author.
E-mail: xiaobao320@163.com

structure can sustain a wide range of stoichiometry as $CaZr_xTi_{3-x}O_7$ with x = 0.80–1.37 [15]. In addition, zirconolite can transform to different polytypes with close structure arrangements, such as 3T (trigonal), 3O (orthorhombic), 2M, and 4M (monoclinic) [16]. The differently coordinated polyhedra enable zirconolite to accommodate large cations into its crystal structure as solid solutions. Naturally existed zirconolite demostrates many different combinations of element substitutions, excellent chemical flexibility, as well as excellent resistance to radiation damage and aqueous dissolution [17]. And zirconolite-based ceramic material has been recognized as one of the most promising matrice phase for nuclear waste disposal [18,19].

In the past, zirconolite-based waste forms were mainly synthesized using traditional methods, such as liquid phase synthesis (hydroxide and sol–gel methods) and solid state reaction sintering [20–22]. These approaches are usually time consuming and costly. High temperature (1400 ℃ or higher) sintering is an indispensable procedure to obtain crystal lattice disposal of actinide-bearing wastes, which inevitably induce the evaporation of volatile nuclides (such as highly radioactive U, Tc, Sr, and Cs elements). Meanwhile, compulsive densification process (such as hot pressing or hot-isostatic pressing) should be conducted to get highly compact samples, which cause the synthesis process more complicated [22]. Recently, reactive spark plasma sintering has been conducted to rapidly synthesize single-phase zirconolite under low temperature (1200 ℃) [23]. Besides that, Muthuraman and his coworkers [24] have proposed combustion synthesis (CS, similar as self-propagating high temperature synthesis, SHS) route for the management of nuclear wastes. Because of the special advantages of high speed, low energy consumption, and simple equipment, the CS technique has been considered as a candidate method for environment protection, such as stabilization of radioactive and toxic wastes [25–27]. It is worth pointing out that the reaction speed and generated temperature of CS can be tailored by adjusting the ingredients of raw reactants. For nuclear waste immobilization, CS route is advantageous for some special applications when the implement environment is confined. Thus, it is valuable to explore the feasibility of zirconolite-based waste forms using the CS process.

In our previous studies, we have investigated the CS preparation of Ce and Nd doped zirconolite-rich waste

forms using $Ca(NO_3)_2$, CuO, MoO_3 as the oxidants and Ti as the reductant [27–30]. CeO_2 has been widely employed as the surrogate of tetravalent actinides (such as Pu and U). However, the incorporated Ce^{4+} is usually reduced to Ce^{3+} under high temperature sintering, as well as the reductive atmosphere of CS process, which leads to that Ce preferentially occupies the Ca site rather than the Zr site of zirconolite [30–32]. From the viewpoint of charge state, Ce is not an ideal surrogate of tetravalent actinides. Actually, Hf is a better simulate element of tetravalent actinides (especially Pu) over Ce as the charge state of Hf^{4+} is very stable. And Hf exhibits identical density and solubility as Pu in the vitrious waste forms [33,34]. On the other hand, Hf is considered as a neutron poison for fission reactions because Hf exhibits much higher thermal neutron capture cross-section than Zr (104 barns for Hf and 0.184 barns for Zr) [35]. Thus, zirconolite-rich ceramics and glass-ceramics with Zr partially or totally substituted by Hf can prevent critical event for the nuclear waste forms heavily loaded with fissile actinide isotopes of ^{239}Pu and ^{235}U [36].

In this study, HfO_2 was employed as the surrogate of tetravalent actinides. As Zr^{4+} and Hf^{4+} cations demonstrate nearly identical ionic radius (0.78 and 0.76 Å for Zr^{4+} and Hf^{4+}, respectively) and belong to the same column in periodic table, these two elements show very close chemical properties and are expected to be incorporated with similar crystal structure [37]. According to charge balance and ionic radius, Hf^{4+} was designed to substitute the Zr site of zirconolite. In order to prepare dense samples, quick pressing (QP) was introduced after the completion of CS reaction. The HfO_2-doped zirconolite-rich waste forms were prepared by the CS/QP process using CuO as the oxidant and Ti as the reductant. The loading capacity of HfO_2 (the x value of $CaZr_{1-x}Hf_xTi_2O_7$) was explored. In addition, the phase composition, site occupancy, densification, and microstructure were investigated. The aqueous durability of representatively solidified Hf-doped sample (Cu-Hf-0.6) was also evaluated using standard Materials Characterization Center (MCC-1) leaching test [38].

2   Experimental details

A series compositions of Hf-doped zirconolite-rich waste forms with the chemical stoichiometry of

$CaZr_{1-x}Hf_xTi_2O_7$ (x = 0.2, 0.4, 0.6, 0.8, 1.0, named as Cu-Hf-0.2 to Cu-Hf-1.0, respectively) were synthesized by CS route. Analytical grade (AR) CuO, CaO, Ti, TiO$_2$, ZrO$_2$, and high purity HfO$_2$ ($\geqslant$ 99.0 wt%) were purchased as the raw materials. The designed CS reactions are demonstrated as follows:

$$2CuO + CaO + Ti + TiO_2 + (1-x)ZrO_2$$
$$+ xHfO_2 \rightarrow CaZr_{1-x}Hf_xTi_2O_7 + 2Cu \qquad (1)$$
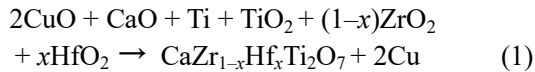
The weight percentages of raw reactants are listed in Table 1, where the yields of Hf-zirconolite are also included. About 20 g raw materials were weighed and sufficiently mixed using agate mortar. The homogenized raw powders were pressed into cylindrical pellets with diameter of 25 mm and height of about 12 mm. The preformed samples were subsequently subjected to CS/QP preparation as illustrated in Fig. 1. The combustion reaction was triggered by a heated tungsten wire, which was motivated by a direct voltage of 30 V and current of 50 A. Silica sand was filled into the stainless steel mould as heat insulator and pressure transmission medium. Before pressure exertion, the combustion temperatures of the samples' center part were measured by a W/Re 5/26 thermocouple, which was connected with an XME2002/U paperless recorder to directly monitor the temperature curve.

The as-synthesized specimens were pulverized into fine powders, which were characterized by X-ray diffractometer (XRD; Rigaku Corporation, Tokyo, Japan) with Cu Kα radiation to obtain the phase compositions. The XRD result of typical Cu-Hf-0.6 sample was subjected to Rietveld refinement using Fullprof-2k software package. After the combustion was finished for 20–30 s, the red-hot samples were pressed by a hydraulic pressure of 45 MPa with 60 s holding time. The finally obtained products with high relative density were sliced and polished on abrasive finishing machine using 0.5 μm diamond pastes. After cleaning and drying, the samples were observed using field-emission scanning electron microscope (FESEM;

Zeiss Ultra-55, Oberkochen, Germany). The phase composition and elemental distribution of solidified Cu-Hf-0.6 sample were analyzed from the results of energy-dispersive X-ray spectrometer (EDX) attached with the FESEM equipment. The chemical durability was evaluated according to the standard MCC-1 leaching test, where the Cu-Hf-0.6 sample was immersed in 90 ℃ deionized water for 1, 3, 7, 14, 21, 28, 35, 42 days, and the leachates were retrieved after each interval. The selected Cu-Hf-0.6 sample was cut and grinded to external dimension of 8.50 mm × 4.78 mm × 4.84 mm. Thus, the specimen surface area to leachate volume ratio (S_A/V value) is 2.62 m^{-1}, which conforms to the requirement of ASTM leaching standard (S_A/V = 0.5–10.0 m^{-1}). Fresh deionized water (80 mL every time) was added to replace the leachate after each interval. The concentrations of Ca and Cu in the leachates were obtained by inductively coupled plasma (ICP) analysis using an iCPA 6500 spectrometer, while Hf was tested by inductively coupled plasma-mass spectrometry (ICP-MS) analysis using an Agilent 7700× spectrometer.

3 Results and discussion

3.1 Combustion temperature and XRD analysis of Hf-doped samples

The combustion experiments of the above-mentioned Hf-doped samples were successfully conducted. The results demonstrate that all the designed green bodies could be ignited by tungsten wire with self-propagation reaction. The combustion reaction lasted for about 10 s after ignition, which means the reaction speed is about 2–3 mm/s. The center temperatures of all these reactions were collected by thermocouple as depicted in Fig. 2. The peak temperatures of these five samples (Cu-Hf-0.2 to Cu-Hf-1.0) are measured to be 1481,

Table 1 Weight percentage of raw reactants for the Hf-doped samples

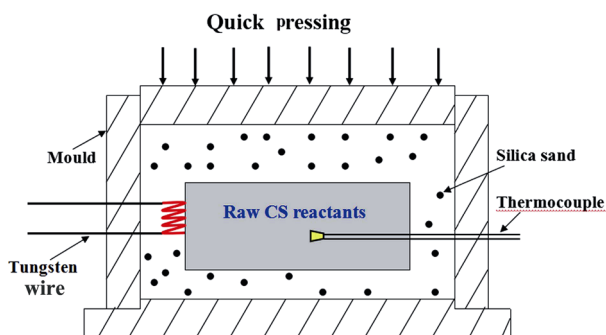| Sample number	Weight percentage of the raw materials (wt%)						Yield of Hf-zirconolite (wt%)	Total (wt%)
	CuO	CaO	Ti	TiO$_2$	ZrO$_2$	HfO$_2$		
Cu-Hf-0.2	43.62	10.24	100	7.30	18.02	7.69	65.16	100
Cu-Hf-0.4	42.28	9.92	100	7.08	13.10	14.91	66.23	100
Cu-Hf-0.6	41.01	9.62	100	6.86	8.47	21.70	67.24	100
Cu-Hf-0.8	39.81	9.34	100	6.67	4.11	28.09	68.20	100
Cu-Hf-1.0	38.68	9.08	100	6.48	0	34.12	69.10	100

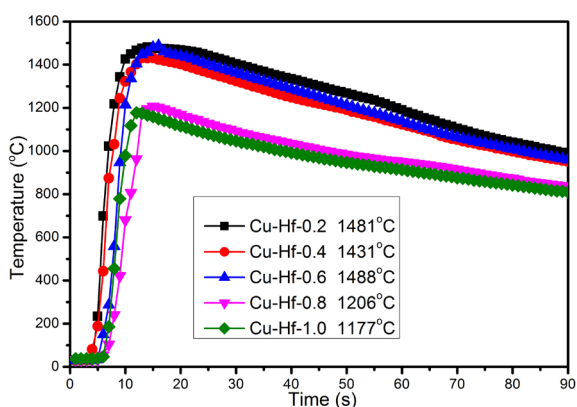**Fig. 1** Schematic diagram of the CS/QP method.

Fig. 2 Combustion temperature of the Hf-doped samples.

1431, 1488, 1206, and 1177 ℃. Compared with the original Zr-zirconolite (1424 ℃) [30], the temperatures of Cu-Hf-0.2, Cu-Hf-0.4, and Cu-Hf-0.6 are slightly higher, while those of Cu-Hf-0.8 and Cu-Hf-1.0 are much lower. Obviously, the decline of peak temperature is attributed to the elevated HfO_2 content. This result reveals that the reactivity of HfO_2 is lower than ZrO_2. As there is heat dissipation during the combustion reaction and subsequent measurement, the real temperatures should be much higher than the measured ones. Anyhow, these temperatures are adequate for subsequent pressing as they are higher than the melting point of resultant Cu (1083 ℃). Because of the existence of liquid Cu, the as-synthesized samples can be readily densified under optimal time delay of combustion.

The phase compositions of Hf-doped samples were characterized with the XRD patterns illustrated in Fig. 3. All these samples show identical phase composition with x value of 0.2–1.0. The phase composition deviates slightly from the original design. 2M-zirconolite ($CaZr_{1-x}Hf_xTi_2O_7$, PDF No. 84-0163) and copper (Cu, PDF No. 99-0034) are identified as the major phases. However, a small amount of perovskite ($CaTiO_3$, PDF

No. 22-0153) is detected as the minor phase, which is also discovered in our previous study [30]. As an important constituent phase of Synroc C, the minor perovskite phase is a valuable supplement of zirconolite for nuclear waste immobilization [22]. The trace of HfO_2 is not detected even in the Cu-Hf-1.0 sample, which indicates HfO_2 has been successfully incorporated into the lattice crystal of ceramic phases as solid solution. The Zr-zirconolite transforms to Hf-zirconolite when the x value is elevated to 1.0. According to the previous study [39], the Zr site of zirconolite could be totally occupied by Hf under solid state reaction route. This result of HfO_2 incorporation is also achieved for the CS process with loading capacity as high as 34.12 wt%. Figure 4 exhibits the refined XRD pattern of Cu-Hf-0.6 sample. This result further testifies the phase composition as Hf-bearing zirconolite, perovskite, and Cu are identified as the constituent phases.
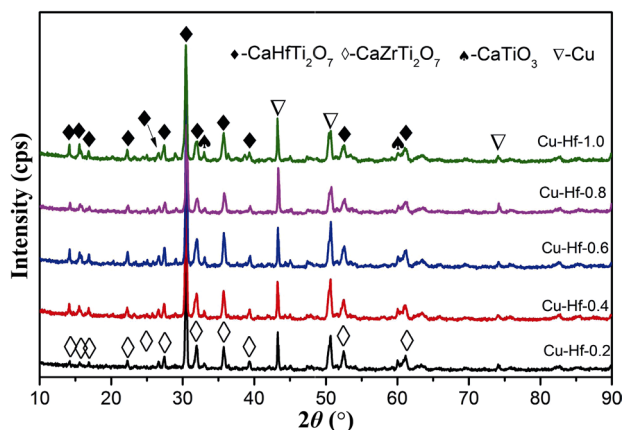

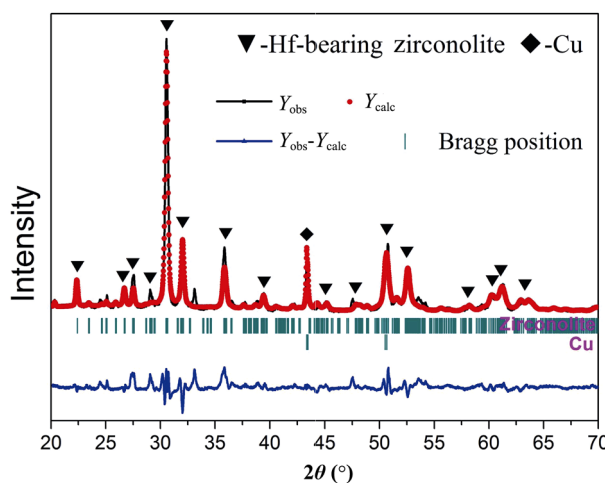**Fig. 3** XRD patterns of the Hf-doped samples with x value of 0.2–1.0.

**Fig. 4** Rietveld refined XRD pattern of the Cu-Hf-0.6 sample.

3. 2　SEM–EDX analysis of the Hf-bearing samples

The phase composition and microstructure of Hf-doped samples (x = 0.2–1.0) were further characterized by the SEM and EDX analysis. Typical back-scattered electron (BSE) images of all the Hf-doped ceramics are shown in Fig. 5. Few micropores can be observed in the surface images, which indicate all the Hf-doped samples were well densified. Meanwhile, three different phases with distinct contrast discrepancies can be detected in the polish surfaces. The metallic Cu always demonstrates circular particle morphology with different size, which is separated from the main ceramic phase with clear grain boundary as shown in Figs. 5(a)–5(e). Besides Cu, the coexistence of two phases can be observed, which are reflected as "Z" and "P" for zirconolite and perovskite phases respectively. The Hf-zirconolite phase is observed with lighter contrast while the pervoskite phase in darker contrast. It is distinctly demonstrated that zirconolite is the matrix phase while perovskite is the dispersion phase. Figure 5(f) is the fracture surface of Cu-Hf-0.6 sample, which exhibits a dense microstructure with tightly contacted submicron sized grains. The growth step can also be observed from the grains, which reveals the feature of combustion synthesis as the reaction speed is high and soaking time is short.

EDX mapping and spotting analysis were conducted to further analyze the phase composition, elemental distribution, and Hf occupation of the Cu-Hf-0.6 sample. The elemental mapping images are presented in Fig. 6. The representative BSE image of Fig. 6(a) supports the coexistence of "A" and "B" phases. Obviously, the "B" area must be Cu phase, which is testified by the EDX mapping image of Fig. 6(e). The "A" phase should be Hf-bearing zirconolite, which

demonstrates as the ceramic matrix. It is worth noting that the enrichment of Cu and Hf elements is slightly overlapped in the same area. Hf not only appears in the matrix A area, but also exists in the Cu phase. This phenomenon is strange as there is no peak corresponding to Hf or HfO$_2$ in the XRD pattern. The subsequent EDX spotting analysis demonstrates that Hf has not been detected in the Cu phase. This phenomenon of Hf in Cu phase is related with the adjacent energy characteristic peaks of Cu and Hf in the EDX analysis (Hf: Kα = 8.040, Kβ = 8.903, Cu: Kα = 7.898, Kβ = 9.021).

EDX spotting analysis was conducted to further determine the chemical formulations of constituent phases. The EDX spotting image of "A" phase in Fig. 6(a) is presented in Figs. 7(a) and 7(b). Similar as the EDX mapping results, the existence of Ca, Ti, Zr, Hf, and O in the EDX spotting spectra indicates that the "A" phase is Hf-bearing zirconolite phase. At least five points of "A" area were calculated to obtain the average elemental quantities as listed in Fig. 7(b). The standard deviations for the average elemental quantities are included in the brackets. Based on this data, the chemical formulation of Hf-bearing zirconolite phase is calculated as Ca$_{0.82}$Zr$_{0.49}$Hf$_{0.68}$Ti$_{1.92}$O$_7$. Compared with the designed formulation of Cu-Hf-0.6 sample (CaZr$_{0.4}$Hf$_{0.6}$Ti$_2$O$_7$), the obtained zirconolite phase is slightly deficient in Ca and Ti while rich in Zr and Hf. This result is reasonable as perovskite is formed as the minor phase. The perovskite phase consumes Ca and Ti elements, which leads to the main zirconolite phase deficient in Ca and rich in Zr. However, the elemental composition is close to the original design and the promising chemical flexibility of zirconolite is verified with the maintaining of 2M zirconolite structure.
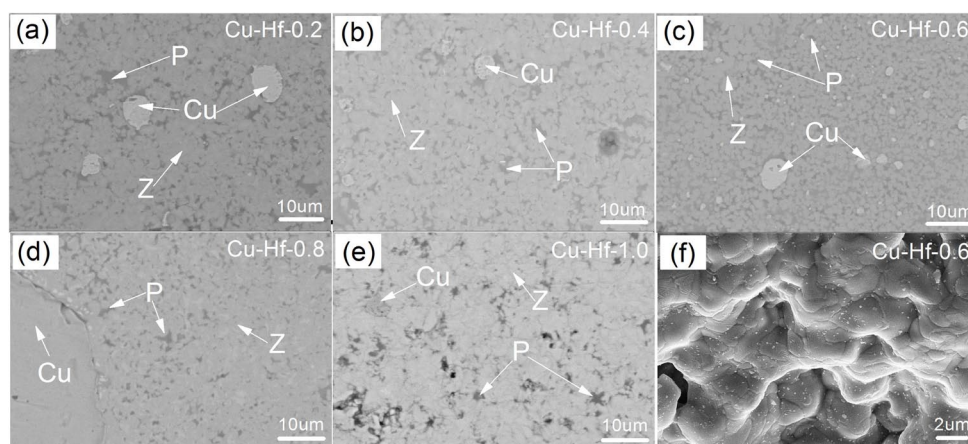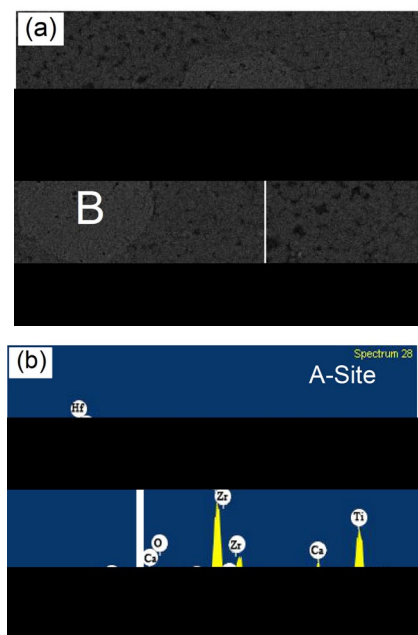

Fig. 5　BSE images of the Hf-doped samples with x = 0.2–1.0: (a) Cu-Hf-0.2, (b) Cu-Hf-0.4, (c) Cu-Hf-0.6, (d) Cu-Hf-0.8, (e) Cu-Hf-1.0, (f) fracture section of the Cu-Hf-0.6 sample.
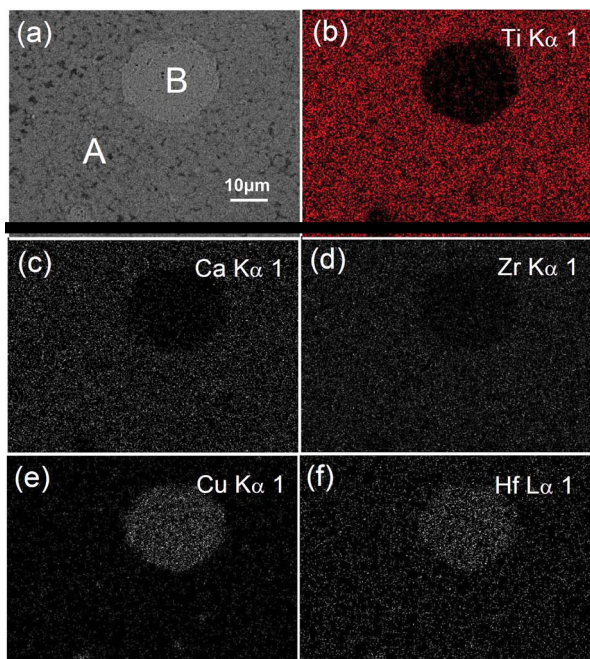
Fig. 6 SEM–EDX mapping images of the Cu-Hf-0.6 sample: (a) representative BSE image, (b)–(f) elemental distribution of Ti, Ca, Zr, Cu, and Hf elements.

Fig. 7 EDX spotting results of Cu-Hf-0.6 sample: (a) representative BSE image, (b) elemental spotting analysis of the "A" region.

3. 3 Chemical stability of the Cu-Hf-0.6 sample

The Cu-Hf-0.6 sample was selected for the standard MCC-1 leaching test. The 1–42-day normalized leaching rates of Ca, Cu, and Hf are measured and illustrated in Fig. 8. With the increase of soaking
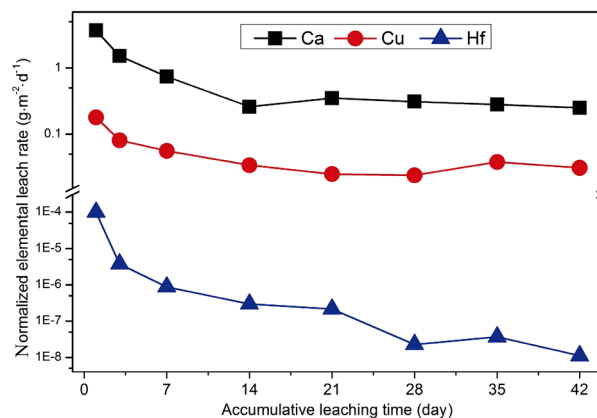
Fig. 8 1–42-day normalized leaching rates of the Cu-Hf-0.6 sample for the Ca, Cu, and Hf elements.

duration, all the normalized leaching rates exhibit a congruent decreasing tendency. The LR_{Ca} and LR_{Cu} values are almost unchanged after 21-day leaching. The 42-day LR_{Ca} and LR_{Cu} are computed to be 0.25 and 3.10×10^{-2} $g \cdot m^{-2} \cdot d^{-1}$. Hf is the most leaching resistant element with the 42-day LR_{Hf} of 1.11×10^{-8} $g \cdot m^{-2} \cdot d^{-1}$. This value is almost the detection limit of ICP-MS. As there is metallic Cu remained in this waste form, the aqueous durability will be affected by this foreign phase. As the existence of Cu has not been considered in the S_A calculation, the leaching surface area of Hf-bearing zirconolite phase should be lower than the computed value. On other words, the actual LR_{Ca} and LR_{Hf} should be slightly higher than the calculated values in Fig. 8, while the LR_{Cu} value should be much lower. Anyhow, the leaching rates of Ca, Cu, and Hf are lower than or comparable to borosilicate glass (about 10^{-2} $g \cdot m^{-2} \cdot d^{-1}$, 90 ℃) [40,41]. Compared with zirconolite and pyrochlore based waste forms prepared by CS, hot pressing (HP), and hot isostatic pressing (HIP) [22,42–45], the leaching rates of Ca and Cu in this research are much higher. Nevertheless, the Hf-bearing zirconolite-rich composite waste form is a durable waste form and the combustion synthesis is a rapid route for nuclear waste disposal.

4 Conclusions

In this study, Hf was employed as the surrogate of tetravalent actinide nuclides. Hf-doped zirconolite-rich composite waste forms were rapidly prepared using CS/QP process. The generated temperature of CS is higher than the melting point of Cu, which leads to liquid phase sintering to obtain highly densified

specimen. The Zr site can be totally occupied by Hf ($x = 1.0$) and the 2M zirconolite structure can be maintained. A small amount of perovskite impurity phase is detected in the final products. The aqueous durability of selected sample (Cu-Hf-0.6) was evaluated, where the 42-day normalized leaching rates (LR_i) of Ca, Cu, and Hf are measured to be 0.25, 3.10×10^{-2}, and 1.11×10^{-8} g·m^{-2}·d^{-1}. These results demonstrate that the CS/QP route is suitable for the preparation of Hf-zirconolite waste forms for the immobilization of HfO$_2$ with loading capacity as high as 34 wt%.

Acknowledgements

References

[1] International Atomic Energy Agency. Design and operation of high level waste. Vitrification and storage facility. Technical Report Series No. 176. IAEA, Vienna, 1977.

[2] Ojovan MI, Lee WE. Principles of nuclear waste management. In: *An Introduction to Nuclear Waste Immobilisation*. Elsevier, 2005: 71–79.

[3] Weber WJ, Navrotsky A, Stefanovsky S, *et al*. Materials science of high-level nuclear waste immobilization. *MRS Bull* 2009, **34**: 46–53.

[4] Ringwood AE, Kesson SE, Ware NG, *et al*. Immobilisation of high level nuclear reactor wastes in SYNROC. *Nature* 1979, **278**: 219–223.

[5] Matzke HJ, Ray ILF, Seatonberry BW, *et al*. Incorporation of transuranic elements in titanate nuclear waste ceramics. *J Am Ceram Soc* 1990, **73**: 370–378.

[6] Lee WE, Gilbert M, Murphy ST, *et al*. Opportunities for advanced ceramics and composites in the nuclear sector. *J Am Ceram Soc* 2013, **96**: 2005–2030.

[7] Vance ER, Ball CJ, Day RA, *et al*. Actinide and rare earth incorporation into zirconolite. *J Alloys Compd* 1994, **213–214**: 406–409.

[8] Ewing RC, Weber WJ, Lian J. Nuclear waste disposal-Pyrochlore (A$_2$B$_2$O$_7$): Nuclear waste form for the immobilization of plutonium and "minor" actinides. *J Appl Phys* 2004, **95**: 5949–5971.

[9] Zhang KB, Wen GJ, Zhang HB, *et al*. Self-propagating high-temperature synthesis of Y$_2$Ti$_2$O$_7$ pyrochlore and its aqueous durability. *J Nucl Mater* 2015, **465**: 1–5.

[10] Peng L, Zhang KB, He ZS, *et al*. Self-propagating high-temperature synthesis of ZrO$_2$ incorporated Gd$_2$Ti$_2$O$_7$ pyrochlore. *J Adv Ceram* 2018, **7**: 41–49.

[11] Zhang KB, He ZS, Peng L, *et al*. Self-propagating synthesis of Y$_{2-x}$Nd$_x$Ti$_2$O$_7$ pyrochlore and its aqueous durability as nuclear waste form. *Scripta Mater* 2018, **146**: 300–303.

[12] Zhang KB, He ZS, Xue JL, *et al*. Self-propagating synthesis of Y$_{2-x}$Nd$_x$Ti$_2$O$_7$ pyrochlores using CuO as the oxidant and its characterizations as waste form. *J Nucl Mater* 2018, **507**: 93–100.

[13] Strachan DM, Scheele RD, Buck EC, *et al*. Radiation damage effects in candidate titanates for Pu disposition: Zirconolite. *J Nucl Mater* 2008, **372**: 16–31.

[14] Cheary RW. Zirconolite CaZr$_{0.92}$Ti$_{2.08}$O$_7$ from 294 to 1173 K. *J Solid State Chem* 1992, **98**: 323–329.

[15] White TJ. The microstructure and microchemistry of synthetic zirconolite, zirkelite and related phases. *Am Mineral* 1984, **69**: 1156–1172.

[16] Coelho AA, Cheary RW, Smith KL. Analysis and structural determination of Nd-substituted zirconolite-4M. *J Solid State Chem* 1997, **129**: 346–359.

[17] Lumpkin GR. Alpha-decay damage and aqueous durability of actinide host phases in natural systems. *J Nucl Mater* 2001, **289**: 136–166.

[18] Ewing RC. Nuclear waste forms for actinides. *P Natl Acad Sci USA* 1999, **96**: 3432–3439.

[19] Vance ER. Synroc: A suitable waste form for actinides. *MRS Bull* 1994, **19**: 28–32.

[20] Jafar M, Sengupta P, Achary SN, *et al*. Phase evolution and microstructural studies in CaZrTi$_2$O$_7$–Nd$_2$Ti$_2$O$_7$ system. *J Am Ceram Soc* 2014, **97**: 609–616.

[21] Teng YC, Wang SL, Huang Y, *et al*. Low-temperature reactive hot-pressing of cerium-doped titanate composite ceramics and their aqueous stability. *J Eur Ceram Soc* 2014, **34**: 985–990.

[22] Zhang Y, Stewart MWA, Li H, *et al*. Zirconolite-rich titanate ceramics for immobilisation of actinides—Waste form/HIP can interactions and chemical durability. *J Nucl Mater* 2009, **395**: 69–74.

[23] Sun SK, Stennett MC, Corkhill CL, *et al*. Reactive spark plasma synthesis of CaZrTi$_2$O$_7$ zirconolite ceramics for plutonium disposition. *J Nucl Mater* 2018, **500**: 11–14.

[24] Muthuraman M, Patil KC, Senbagaraman S, *et al*. Sintering, microstructural and dilatometric studies of combustion synthesized synroc phases. *Mater Res Bull* 1996, **31**: 1375–1381.

[25] Barinova TV, Borovinskaya IP, Ratnikov VI, *et al*. SHS immobilization of radioactive wastes. *Key Eng Mater* 2001, **217**: 193–200.

[26] Cao G, Orrù R. Self-propagating reactions for environmental protection: State of the art and future directions. *Chem Eng J* 2002, **87**: 239–249.

[27] Mao XH, Qin ZG, Yuan XN, *et al*. Immobilization of

simulated radioactive soil waste containing cerium by self-propagating high-temperature synthesis. *J Nucl Mater* 2013, **443**: 428–431.

[28] Zhang KB, Yin D, Han PW, *et al*. Two-step synthesis of zirconolite-rich ceramic waste matrice and its physicochemical properties. *Int J Appl Ceram Technol* 2018, **15**: 171–178.

[29] Zhang KB, Wen GJ, Zhang HB, *et al*. Self-propagating high-temperature synthesis of CeO_2 incorporated zirconolite-rich waste forms and the aqueous durability. *J Eur Ceram Soc* 2015, **35**: 3085–3093.

[30] Zhang KB, Yin D, Peng L, *et al*. Self-propagating synthesis and CeO_2 immobilization of zirconolite-rich composites using CuO as the oxidant. *Ceram Int* 2017, **43**: 1415–1423.

[31] Szajman J, Smart RSC, Myhra S. X-ray photoelectron spectroscopy studies of valence states of cerium and uranium in SYNROC C. *Surf Coat Technol* 1987, **30**: 333–342.

[32] Holgado JP, Alvarez R, Munuera G. Study of CeO_2 XPS spectra by factor analysis: Reduction of CeO_2. *Appl Surf Sci* 2000, **161**: 301–315.

[33] Cachia JN, Deschanels X, den Auwer C, *et al*. Enhancing cerium and plutonium solubility by reduction in borosilicate glass. *J Nucl Mater* 2006, **352**: 182–189.

[34] Curti E, Grolimund D, Borca CN. A micro-XAS/XRF and thermodynamic study of $Ce^{III/IV}$ speciation after long-term aqueous alteration of simulated nuclear waste glass: Relevance for predicting Pu behavior? *Appl Geochem* 2012, **27**: 56–63.

[35] Emsley J. *The Elements*. Oxford: Clarendon Press, 1992.

[36] Perera DS, Stewart MWA, Li HJ, *et al*. Tentative phase relationships in the system $CaHfTi_2O_7$–$Gd_2Ti_2O_7$ with up to 15 mol% additions of Al_2TiO_5 and $MgTi_2O_5$. *J Am Ceram Soc* 2004, **85**: 2919–2924.

[37] Shannon RD. Revised effective ionic radii and systematic studies of interatomic distances in halides and chalcogenides. *Acta Cryst* 1976, **A32**: 751–767.

[38] ASTM C1220-98. Standard test method for static leaching of monolithic waste forms for disposal of radioactive waste. West Conshohocken, PA, USA, 1998.

[39] Caurant D, Loiseau P, Bardez I. Structural characterization of Nd-doped Hf-zirconolite $Ca_{1-x}Nd_xHfTi_{2-x}Al_xO_7$ ceramics. *J Nucl Mater* 2010, **407**: 88–99.

[40] Smith KL, Lumpkin GR, Blackford MG, *et al*. The durability of synroc. *J Nucl Mater* 1992, **190**: 287–294.

[41] Guittonneau C, Gin S, Godon N, *et al*. A 25-year laboratory experiment on French SON68 nuclear glass leached in a granitic environment—First investigations. *J Nucl Mater* 2011, **408**: 73–89.

[42] Teng YC, Wang SL, Huang Y, *et al*. Low-temperature reactive hot-pressing of cerium-doped titanate composite ceramics and their aqueous stability. *J Eur Ceram Soc* 2014, **34**: 985–990.

[43] Cai X, Teng YC, Wu L, *et al*. The synthesis and chemical durability of Nd-doped single-phase zirconolite solid solutions. *J Nucl Mater* 2016, **479**: 455–460.

[44] He ZS, Zhang KB, Peng L, *et al*. Self-propagating plus quick pressing synthesis and characterizations of $Gd_{2-x}Nd_xTi_{1.3}Zr_{0.7}O_7$ ($0 \leqslant x \leqslant 1.4$) pyrochlores. *J Nucl Mater* 2018, **504**: 61–67.

[45] He ZS, Zhang KB, Xue JL, *et al*. Self-propagating chemical furnace synthesis of nanograin $Gd_2Zr_2O_7$ ceramic and its aqueous durability. *J Nucl Mater* 2018, **512**: 385–390.